

Nuclear Structure Properties and Stellar Weak Rates for ^{76}Se : Unblocking of the Gamow Teller Strength

Jameel-Un Nabi¹, Mavra Ishfaq¹, Mahmut Büyükata², Muhammad Riaz¹

¹*Faculty of Engineering Sciences, GIK Institute of Engineering Sciences and Technology, Topi 23640, Swabi, Khyber Pakhtunkhwa, Pakistan*

²*Physics Department, Science and Arts Faculty, Kırıkkale University, 71450, Kırıkkale, Turkey*

Abstract

At finite temperatures ($\geq 10^7\text{K}$), ^{76}Se is abundant in the core of massive stars and electron capture on ^{76}Se has a consequential role to play in the dynamics of core-collapse. The present work may be classified into two main categories. In the first phase we study the nuclear structure properties of ^{76}Se using the interacting boson model-1 (IBM-1). The IBM-1 investigations include the energy levels, $B(E2)$ values and the prediction of the geometry. We performed the extended consistent- Q formalism (ECQF) calculation and later the triaxial formalism calculation (constructed by adding the *cubic* term to the ECQF). The geometry of ^{76}Se can be envisioned within the formalism of the potential energy surface based on the classical limit of IBM-1 model. In the second phase, we reconfirm the unblocking of the Gamow-Teller (GT) strength in ^{76}Se (a test case for nuclei having $N > 40$ and $Z < 40$). Using the deformed pn-QRPA model we calculate GT transitions, stellar electron capture cross section (within the limit of low momentum transfer) and stellar weak rates for ^{76}Se . The distinguishing feature of our calculation is a state-by-state evaluation of stellar weak rates in a fully microscopic fashion. Results are compared with experimental data and previous calculations. The calculated GT distribution fulfills the Ikeda sum rule. Rates for β -delayed neutrons and emission probabilities are also calculated. Our study suggests that at high stellar temperatures and low densities, the β^+ -decay on ^{76}Se should not be neglected and needs to be taken into consideration along with electron capture rates for simulation of presupernova evolution of massive stars.

Keywords: Gamow-Teller transitions; pn-QRPA model; IBM model; nuclear structure; triaxiality; cubic interactions; electron capture; β -delayed neutron emissions.

1. Introduction

It is well known that electron captures on nuclei have a decisive role during the end stages of presupernova and supernova phases of massive stars [1, 2]. Capturing of electrons reduces the degenerate relativistic electron gas pressure and ultimately leads to the gravitational collapse of the core of a massive star. The electron capture process also assists in reducing the electron-to-baryon content, tilting the stellar matter towards more neutron rich (hence heavy) nuclei. Some notable mentions of past electron capture rate calculations include [3] (based on relativistic energy density functionals), [4, 5] (based on Skyrme finite temperature RPA), [6] (FRDM + RPA), [7] (QRPA with separable interaction and deformed single particle potential), [8] (continuum QRPA + density functional theory) [9] (large scale shell model calculation), [10] (shell model Monte Carlo method) and [11] (shell model). See also Table 1 of Ref. [8] for a list of global microscopic approaches to the calculation of weak rates. In this paper we signify the transformation of a proton into a neutron by GT_+ transitions.

Within the same major shell, the Independent Particle Model (IPM) forbids the conversion of protons into neutrons for $Z < 40$ and $N > 40$. This is due to the Pauli blocking of the Gamow-Teller (GT) transitions. However it was debated that nuclear correlation effects can make such transitions possible if nucleons are allowed to move from one major shell (fp -shell) to another (sdg -shell). Also environments with finite temperature (as in core of massive stars) can assist in doing the needful transformation. In order to study the unblocking of GT strength with the help of finite temperature and nuclear correlation effects, we select the nucleus ^{76}Se in this paper. This nucleus is also chosen because of its copious production in the stellar core, during the presupernova and supernova phases, of massive stars. The calculated GT strength distribution is sensitive to nuclear structure properties, specially the deformation parameter (β_2). In order to study the nuclear structure properties of ^{76}Se , we chose the interacting boson model-1 (IBM-1) [12]. The structure of ^{76}Se and its neighboring isotopes were previously studied within the interacting boson model-2 (IBM-2) [12] where the neutron and the proton bosons were separately taken into account (e.g. [13, 14, 15, 16, 17]). These

studies were mostly performed at low energy levels. Along $Z = 32$ isotopic chain, the sub-shell effects were studied in Ref. [13] where it was concluded that the sub-shell effect occurs for $N \leq 40$ in spite of the absence of this effect for $N \geq 42$. Radhi and Stewart focused on the mixed-symmetry states at low-spin level scheme of ^{76}Se [14] within the concept of F-spin in the framework of IBM-2. To identify the effects of the shell closure $N = 50$, the g factors of the 0_{β}^{+} , 2_{γ}^{+} , 4_{gs}^{+} triplet states, appearing along the stable $^{74-82}\text{Se}$ isotopes, were experimentally measured and compared with the IBM-2 results [15]. The energy levels, B(E2) and B(M1) transition probabilities of this isotopic chain were investigated in detail by using different sets of IBM-2 Hamiltonian parameters in recent works [16, 17].

The present work can be divided into two main phases. In the first phase, because of the behavior of ^{76}Se , two kinds of IBM-1 calculation were performed to analyze its structural properties. This nucleus looks spherical since the phonon multiplets picture occurs as (0_{gs}^{+}) , (2_{gs}^{+}) , $(4_{gs}^{+}, 2_{\gamma}^{+}, 0_{\beta}^{+})$, $(6_{gs}^{+}, 3_{\gamma}^{+}, 2_{\beta}^{+})$, ... at the low energy spectra. Despite this spherical behavior, its energy ratio in the ground state band is $R_{4/2} = 2.38$ (located in between $R_{4/2}^{U(5)} = 2.00$ and $R_{4/2}^{O(6)} = 2.50$, which are the typical ratios of the spherical and the γ -softness cases, respectively). To move in between U(5) and O(6) symmetries, we chose the extended consistent- Q formalism (ECQF) [18] for the *first* calculation. We also performed the *second* calculation by adding the *cubic* term [19] to the ECQF Hamiltonian to study its effect on the energy levels in γ -band. The $B(E2)$ values were also calculated and compared with experimental data for ^{76}Se . After complete parametrization of the Hamiltonian, the geometry of ^{76}Se was predicted by plotting potential energy surface as a function of deformation parameters (β, γ) within the two formalisms of IBM-1. In the second phase, the IBM-1 (triaxial formalism calculation) energy levels were used as parent excited states of ^{76}Se to calculate stellar weak rates using the the proton-neutron quasiparticle random phase approximation (pn-QRPA) model [20].

It is no surprise that different theoretical models have been used in the past to calculate weak rates in stellar matter. There are two major issues in calculation of stellar weak rates. There are hundreds of nuclear species present in the stellar matter and ideally one would like to calculate weak rates for all these nuclei. The second problem is even more challenging. High temperatures prevailing in the stellar matter populate parent excited states and the total weak rate has a finite contribution from these excited

states. Most of the nuclear models would calculate ground state GT_+ distributions (and maybe also for a few low-lying parent states) and then adopt the so-called Brink-Axel hypothesis (BAH) [21] for high-lying energy levels. BAH states that the GT resonance resides at the same relative energy in daughter for all parent excited states akin to the ground state. Special mention of weak rate calculations covering a wide range of nuclei would include the IPM calculation [22, 23], the pn-QRPA [24, 25, 26] calculation and the large scale shell model (LSSM) [27] calculation. The pn-QRPA model, when used with a schematic separable interaction, has a distinguishing feature. It allows a state-by-state calculation of ground state and *all* excited states GT distributions in a microscopic fashion. In other words BAH is not assumed in the pn-QRPA calculation (it is used in the IPM and LSSM calculation). The reliability of pn-QRPA calculation hence increases many fold as excited states contribute effectively to the total weak rate in the core of massive stars. The pn-QRPA model also possesses the additional advantage that it can be employed for any arbitrarily heavy system of nucleons.

Previous works [28, 29] where both IBM-1 and pn-QRPN calculations were put into action were performed for the waiting point (WP) nuclei ^{60}Zn , ^{64}Ge , ^{68}Se , ^{72}Kr , ^{76}Sr , ^{80}Zr , ^{84}Mo , ^{88}Ru , ^{92}Pd and ^{96}Cd along $N = Z$ chain. These included the investigations of the nuclear structure properties and their geometries. All these nuclei were exotic (short live nuclei) and displayed varying behavior along the line. $B(E2:2_1^+ \rightarrow 0_1^+)$ was experimentally detected for only two nuclei; ^{68}Se and ^{72}Kr . Unlike the past exotic nuclei, ^{76}Se , considered in this paper, is a stable nucleus and has enough relevant experimental data. Further one of the main aims of the current work is to study the unblocking of GT strength.

The Pauli blocking mechanism of allowed neutron hole orbits available via the GT operator to protons capturing electrons in the IPM was discussed in length by Fuller [23]. It was concluded that capture on free protons dominates the neutronization rate in this region. It was later argued that Pauli blocking would be overcome by finite temperature and nuclear correlations effects [30]. GT transitions are thermally unblocked primarily as a result of the excitation of neutrons from the fp shell into the $g_{9/2}$ orbital. This unblocking allows GT transitions within the fp shell, leading to domination of electron capture rates on nuclei rather than free protons [31], in contradiction to previous findings. On the other hand, Cooperstein and Wambach [32] noted, from an investigation based on the random phase approximation, that electron capture on neutron-rich nuclei with protons in the fp shell and $N >$

40 can compete with capture on free protons if one considers forbidden transitions in addition to allowed ones. The unblocking of GT strength in ^{76}Se was experimentally verified independently by (d, ^2He) charge-exchange reaction experiment at KV1 Groningen [33] and by the (n, p) reaction at TRIUMF [34]. Different theoretical models also confirmed this unblocking by calculating GT_+ transitions for ^{76}Se . Here we would like to mention the deformed pn-QRPA calculation with density-dependent Skyrme forces [35], LSSM [36] and deformed QRPA calculation using a realistic two-body interaction [37]. Theoretical calculations on unblocking of GT strength are also available in literature where other test cases were studied. In the second phase of this paper, we use the pn-QRPA in a multi-shell deformed single-particle space with a schematic separable interaction to calculate GT_+ transitions in ^{76}Se and reconfirm the unblocking of GT strength for nuclei having $N > 40$ and $Z < 40$. We later extend this model to calculate weak-interaction mediated rates in stellar matter for ^{76}Se .

Our paper is organized as follows. Section 2 briefly discusses the necessary formalism of the IBM-1 and the pn-QRPA models used in our calculation. Section 3 discusses and compares our calculation with measured data and previous theoretical results. Section 4 finally summarizes our findings.

2. Formalism

2.1. Interacting Boson Model-1 (IBM-1)

The IBM-1 model is one of the powerful approaches to study nuclear structure properties of even-even nuclei. This model is a group theoretical approach and is established on unitary algebra $U(6)$. The $U(6)$ group has three possible sub-algebras denoted by $U(5)$, $SU(3)$ and $O(6)$ known as *Dynamical Symmetries* [38]. In the IBM-1 model, different versions of the Hamiltonian can be formulated depending on the behavior of the given nucleus. The simple one is the consistent- Q formalism (CQF) [39, 40] including only two terms $\hat{Q} \cdot \hat{Q}$ and $\hat{L} \cdot \hat{L}$ and the Hamiltonian can be written as

$$\hat{H}_{CQF} = a_1 \hat{L} \cdot \hat{L} + a_2 \hat{Q} \cdot \hat{Q}. \quad (1)$$

Here, \hat{L} and \hat{Q} are the angular momentum and quadrupole operators, respectively, as defined by $\hat{L} = \sqrt{10}[d^\dagger \times \tilde{d}]^{(0)}$, $\hat{Q} = [d^\dagger \times \tilde{s} + s^\dagger \times \tilde{d}]^{(2)} + \bar{\chi}[d^\dagger \times \tilde{d}]^{(2)}$. The extended version of this simple Hamiltonian is called the extended consistent- Q formalism (ECQF) [18] and is formed by adding an extra term \hat{n}_d to the

CQF Hamiltonian in Eq. (1). The ECQF formalism provides the advantage to reach all three symmetries and to move in between three dynamical symmetries. The ECQF Hamiltonian [18] with three terms is written as follows

$$\hat{H}_{ECQF} = \epsilon_d \hat{n}_d + a_1 \hat{L} \cdot \hat{L} + a_2 \hat{Q} \cdot \hat{Q}, \quad (2)$$

where, \hat{n}_d is the boson-number defined by $\hat{n}_d = \sqrt{5}[d^\dagger \times \tilde{d}]^{(0)}$. The constants ϵ_d , a_1 , a_2 are free parameters. These are fitted to experimental data taken from National Nuclear Data Center (NNDC) [41]. Hamiltonian (2) includes *four* parameters in total with $\bar{\chi}$ given in the quadrupole operator \hat{Q} . In addition to the energy levels, the $B(E2)$ values can be calculated in IBM-1 model by using the $E2$ operator $\hat{T}(E2) = e_b \hat{Q}$, where e_b is the boson effective charge.

The triaxial formalism of IBM-1 was obtained by adding the *cubic* interaction (also known as the *three – body* term) to the given Hamiltonian for triaxial effect in the IBM-1 as discussed in detail in Refs. [19, 42]. Some of the $O(6)$ like nuclei were investigated within this formalism in Refs. [43, 44]. For the second calculation of the present application, we formulate the triaxial case by adding this *cubic* term to the ECQF Hamiltonian (2), like in [19], as following

$$\hat{H} = \hat{H}_{ECQF} + \sum_L v_L [d^\dagger d^\dagger d^\dagger]^{(L)} \cdot [\tilde{d}\tilde{d}\tilde{d}]^{(L)}. \quad (3)$$

The useful way to understand the effect of this *cubic* term in the γ band is to look for the signature splitting of the γ band $S(J)$ [45]. One can test the γ -softness behavior within the given formula in [46, 47] as

$$S(J) = \frac{E(J) - E(J-1)}{E(J) - E(J-2)} \cdot \frac{J(J+1) - (J-1)(J-2)}{J(J+1) - J(J-1)} - 1, \quad (4)$$

which describes whether the even–odd staggering appears in the γ band. In recent works [46, 47], transitional nuclei situated in between the spherical and γ -unstable cases were studied within the triaxial formalism based on a Hamiltonian with three–body term. Fortunato *et. al.* [48] added this term in the Hamiltonian of the CQF to find the phase space of the triaxial region in between the oblate and prolate shapes.

The other useful way for prediction of the nuclear shape is to plot the potential energy surface $V(\beta, \gamma)$ obtained from the IBM-1 Hamiltonian in

the classical limit [49, 50, 51]. The energy surface was found as in Ref. [47]

$$V(\beta, \gamma) = E_0 + \sum_{n \geq 1} \frac{N(N-1) \cdots (N-n+1)}{(1+\beta^2)^n} \sum_{kl} a_{kl}^{(n)} \beta^{2k+3l} \cos^l 3\gamma, \quad (5)$$

where the constant E_0 represents the binding energy of the core. This energy surface can be written with the factors $a_{kl}^{(n)}$, where $n = 1, 2, 3$ indicates the order of the interaction in the generators of $U(6)$:

$$\begin{aligned} V(\beta, \gamma) = & \frac{N}{1+\beta^2} (a_{00}^{(1)} + a_{10}^{(1)} \beta^2) + \\ & \frac{N(N-1)}{(1+\beta^2)^2} (a_{00}^{(2)} + a_{10}^{(2)} \beta^2 + a_{01}^{(2)} \beta^3 \cos 3\gamma + a_{20}^{(2)} \beta^4) + \\ & \frac{N(N-1)(N-2)}{(1+\beta^2)^3} (a_{00}^{(3)} + a_{10}^{(3)} \beta^2 + a_{01}^{(3)} \beta^3 \cos 3\gamma + a_{11}^{(3)} \beta^5 \cos 3\gamma + a_{20}^{(3)} \beta^4 + a_{02}^{(3)} \beta^6 \cos^2 3\gamma + a_{30}^{(3)} \beta^6) \end{aligned}$$

The factors $a_{kl}^{(n)}$ ($n = 1, 2, 3$) are also referred to as *one-body*, *two-body*, and *three-body* interactions, respectively, as discussed in detail in Ref. [47]. Here, it can be reduced for Hamiltonian (2) as follows

$$V(\beta, \gamma) = \epsilon N \frac{\beta^2}{1+\beta^2} + a_2 N(N-1) \left[\frac{5 + (1 + \overline{\chi}^2) \beta^2}{(N-1)(1+\beta^2)} + \frac{\left(\frac{2\overline{\chi}^2 \beta^4}{7} - 4\sqrt{\frac{2}{7}} \overline{\chi} \beta^3 \cos(3\gamma) + 4\beta^2 \right)}{(1+\beta^2)^2} \right], \quad (7)$$

which includes common free parameters used as constant in the *ECQF* formalism. By adding the *cubic* interaction, we can obtain the energy surface for triaxial formalism as

$$\begin{aligned} V(\beta, \gamma) = & \epsilon N \frac{\beta^2}{1+\beta^2} + \\ & a_2 N(N-1) \left[\frac{5 + (1 + \overline{\chi}^2) \beta^2}{(N-1)(1+\beta^2)} + (N-1) \frac{\left(\frac{2\overline{\chi}^2 \beta^4}{7} - 4\sqrt{\frac{2}{7}} \overline{\chi} \beta^3 \cos(3\gamma) + 4\beta^2 \right)}{(1+\beta^2)^2} \right] + \\ & v_3 N(N-1)(N-2) \frac{1}{30(1+\beta^2)^3} \sin^2 3\gamma, \end{aligned} \quad (8)$$

where the *cubic* interaction with $L = 3$ is symbolized by v_3 and it is commensurate to $\sin^2 3\gamma (= 1 - \cos^2 3\gamma)$.

Both formalisms of the energy surface given in Eqs. (7) and (8) include the shape variables (β, γ) , also known as deformation parameters. These variables have similar role as in the collective model of Bohr and Mottelson [52]. The role of these collective deformations is that β measures the axial deviation from sphericity and the angle γ controls the departure from axial deformation. Within the energy surface of IBM-1, one can move in between the three dynamical symmetries relating to the geometry of nuclei. The $U(5)$, $SU(3)$ and $O(6)$ symmetries correspond to the spherical, the axially deformed and γ -unstable shapes, respectively.

2.2. The pn-QRPA formalism for calculation of stellar weak rates

The Hamiltonian of the pn-QRPA model was chosen as

$$H^{QRPA} = H^{sp} + V^{pair} + V_{GT}^{ph} + V_{GT}^{pp}. \quad (9)$$

Wave functions and single particle energies were calculated using the Nilsson model (axially deformed). Pairing in nuclei was treated within the BCS approximation. The proton-neutron residual interaction occurred through particle-particle (pp) and particle-hole (ph) channels in our model. In the pn-QRPA model these interaction (force) terms were given a separable form as V_{GT}^{ph} for the particle-hole Gamow-Teller force and V_{GT}^{pp} for the particle-particle Gamow-Teller force. The other parameters for calculation of weak rates are the Nilsson potential parameters, the pairing gaps, the nuclear quadrupole deformation, and the Q-value of the reaction. Nilsson-potential parameters were adopted from Ref. [53] and the Nilsson oscillator constant was chosen as $\hbar\omega = 41A^{-1/3}(MeV)$ (the same for protons and neutrons). Pairing gaps used in the present work were taken as $\Delta_p = \Delta_n = 12/\sqrt{A}(MeV)$. Nuclear quadrupole deformation parameter selection would be discussed in Section 3. Q-values were taken from the recent mass compilation of Audi and collaborators [54].

Calculation of stellar weak rates using the pn-QRPA model was first performed by Nabi et al. [24]. The decay rate from parent state (i th) to the daughter state (j th) of the nucleus is given by

$$\lambda_{ij}^{ec(pd)} = \ln 2 \frac{f_{ij}^{ec(pd)}}{(ft)_{ij}^{ec(pd)}}. \quad (10)$$

The $f_{ij}^{ec(pd)}$ are the phase space integrals for electron capture (positron decay) reaction and are functions of stellar temperature (T), density (ρ) and Fermi energy (E_f) of the leptons. They are explicitly given by

$$f_{ij}^{ec} = \int_{w_l}^{\infty} w \sqrt{w^2 - 1} (w_m + w)^2 F(+Z, w) G_- dw. \quad (11)$$

and by

$$f_{ij}^{pd} = \int_1^{w_m} w \sqrt{w^2 - 1} (w_m - w)^3 F(-Z, w) (1 - G_+) dw, \quad (12)$$

In Eqs. (11) and (12), w is the total energy of the electron including its rest mass. w_m is the total β -decay energy,

$$w_m = m_p - m_d + E_i - E_j, \quad (13)$$

where m_p and E_i are masses and excitation energies of the parent nucleus, and m_d and E_j of the daughter nucleus, respectively. $F(\pm Z, w)$ are the Fermi functions and were calculated according to the procedure adopted by Gove and Martin [55]. G_{\pm} are the Fermi-Dirac distribution functions for positrons (electrons).

The ft values are associated with the reduced transition probability of nuclear transitions B_{ij} ,

$$(ft)_{ij}^{ec(pd)} = F/B_{ij}. \quad (14)$$

The F in Eq. 14 represents a physical constant,

$$F = \frac{2 \ln 2 \hbar^7 \pi^3}{g_V^2 m_e^5 c^4}, \quad (15)$$

with a value of $6146 \pm 6s$ [56], and

$$B_{ij} = B(F)_{ij} + (g_A/g_V)^2 B(GT)_{ij}, \quad (16)$$

$$B(F)_{ij} = \frac{1}{2J_i + 1} |\langle j || \sum_k t_+^k || i \rangle|^2, \quad (17)$$

$$B(GT)_{ij} = \frac{1}{2J_i + 1} |\langle j || \sum_k t_+^k \vec{\sigma}^k || i \rangle|^2. \quad (18)$$

The value of the ratio of axial to vector coupling constant (g_A/g_V) was taken as - 1.2694 [57]. In Eq. 18, t_+^k shows isospin raising operator while $\vec{\sigma}^k$ represents the spin operator.

The total electron capture/ β^+ decay rate per unit time per nucleus is finally given by

$$\lambda^{ec(pd)} = \sum_{ij} P_i \lambda_{ij}^{ec(pd)}. \quad (19)$$

The summation was performed until satisfactory convergence was achieved in our rate calculation. The occupation probability of a given parent excited state, P_i , was calculated assuming the Boltzmann distribution.

In our calculation it was further assumed that daughter excited states, having energy larger than separation energy for neutrons (S_n), would decay by emission of neutrons. From the daughter nucleus the rate of neutron energy was calculated using the relation

$$\lambda^n = \sum_{ij} P_i \lambda_{ij} (E_j - S_n), \quad (20)$$

for all $E_j > S_n$.

The β -delayed neutron emission probability was calculated using

$$P^n = \frac{\sum_{ijj'} P_i \lambda_{ijj'}}{\sum_{ij} P_i \lambda_{ij}}, \quad (21)$$

here j' are the daughter states for which $E_{j'} > S_n$. In Eqs. (20 and 21), $\lambda_{ij(i)}$, for the transition $i \rightarrow j(j')$, is sum of electron capture and positron decay rates.

The Q-values, adopted in our calculation, were taken from the recent mass compilation of Audi et al. [54].

The pn-QRPA results for calculated GT strength was quenched by a factor of $f_q^2 = (0.55)^2$ [58]. The re-normalized Ikeda sum rule translates to

$$(ISR)_{renorm} = \sum B(GT)_- - \sum B(GT)_+ \cong 3f_q^2(N - Z). \quad (22)$$

The difference in our calculated (and quenched) strength values was 7.14. This was very close to the re-normalized Ikeda sum rule value of 7.26. The 98.34% fulfillment of Ikeda sum rule deserves a special mention in this work.

For details of the pn-QRPA model Hamiltonian and solution of the QRPA equation with separable GT forces we refer to [59].

2.3. Electron capture cross sections

The nucleus (N, Z) captures electron of incident energy (E_e) and decay weakly as

$$(N, Z) + e^- \longrightarrow (N + 1, Z - 1)^* + \nu_e \quad (23)$$

The incident electron energy maybe distributed into two parts, a part of it is absorbed by daughter nucleus ($N + 1, Z - 1$) to change its state from initial E_i to final E_f state and the remaining energy is carried out by neutrino ν_e .

Using energy conservation in Eq. (23), the energy of the outgoing neutrino E_ν may be calculated using

$$E_\nu = E_e - Q + E_i - E_f, \quad (24)$$

where the Q value is simply the difference of the measured masses of parent and daughter nuclei. The nuclear reaction cross section calculation for the reaction (23) is governed by the weak Hamiltonian

$$\hat{H} = \frac{G}{\sqrt{2}} j_\mu^{lept} \hat{J}^\mu, \quad (25)$$

where $G = G_F \cos\theta_c$, G_F is the Fermi coupling constant, θ_c is Cabibbo angle, j_μ^{lept} and \hat{J}^μ are the leptonic and hadronic currents, respectively (for further details, see e.g. [60]).

We used the limiting condition $q \rightarrow 0$ of low momentum transfer. Using this assumption the impact on the total electron capture cross section is provided only by the GT transitions [61]. The pn-QRPA calculated energy eigenvalues of the parent nucleus $|i\rangle$ were replaced manually by those calculated using the IBM-1 calculation (triaxial formalism). The excited states of daughter nucleus $|f\rangle$ and GT transitions were calculated using the pn-QRPA equations with separable GT forces [59]. The total stellar EC cross section, as a function of incident electron energy and stellar temperature, is given by

$$\begin{aligned} \sigma(E_e, T) = & \frac{G_F^2 \cos^2\theta_c}{2\pi} \sum_i F(Z, E_e) \frac{(2J_i + 1) \exp(-E_i/kT)}{G(A, Z, T)} \\ & \times \sum_{J,f} (E_e - Q + E_i - E_f)^2 \frac{|\langle i | \sigma\tau_+ | f \rangle|^2}{(2J_i + 1)}. \end{aligned} \quad (26)$$

In Eq. (26), $F(Z, E_e)$ is the well known Fermi function and was calculated according to the prescription given in Ref [55]. $G(A, Z, T)$ are the nuclear partition functions and were calculated using the recipe of [62].

3. Results and Discussions

The energy spectra of ^{76}Se were calculated by fitting the Hamiltonian parameters in Eqs. (2) and (3). This spectra includes 17 experimentally known levels in the ground state (*g.s.*), γ and β bands [41]. In addition to the calculation of the known levels, the prediction was also made for unknowns

in the γ and β bands. For this application, we performed two calculations; the *first* one is denoted by IBM-1 for the EQCF formalism and the *second* by IBM-1* with *star* for the formalism in Eq. (3) including *cubic* term.

For the fitting procedure of the *first* calculation, we first determined ϵ_d while keeping other constants as *zero*. Later we fitted the other two parameters (a_2, a_1) by minimizing the root-mean-square (*rms*) deviation. Finally, $\bar{\chi}$ was determined by changing its value from 0 to $-\sqrt{7}/2$, step by step, and for each step ϵ_d, a_2, a_1 were re-fitted to find minimum *rms* value (see Table 1). The calculated energy levels (dotted lines) with IBM-1 (EQCF) and the experimental data (bold lines) are illustrated in Fig. 1. As seen in this figure, the IBM-1 results are in good agreement especially for the levels in *g.s.* and β bands except for the levels in γ band. An important feature of abnormal levels called "staggering" appears in γ band. The calculated γ band levels tend to be coupled as $(2_\gamma^+), (3_\gamma^+, 4_\gamma^+), (3_\gamma^+, 4_\gamma^+), (5_\gamma^+, 6_\gamma^+), \dots$; a typical band structure of the γ -softness [63]. However, these couplings are not so close for experimental data and it is difficult to predict whether ^{76}Se exhibit exact γ -softness picture. Nevertheless, this result gives a choice to test the effect of *cubic* term on the γ band levels. Later we added the *cubic* term to the Hamiltonian (2) for the *second* calculation shown as IBM-1*. We carried out a similar fitting procedure as for the *first* calculation to determine the parameters of the Hamiltonian (3). As a result, we obtained a smaller *rms* value as given in Table 1 and this suggests that the *cubic* term has a positive effect on the γ band levels. The *second* calculated levels (dashed lines) of *g.s.* and β bands are the same as the *first* one. The γ band levels appear better in the triaxial formalism since the odd-even couplings are separated as seen in Fig. 1.

Another useful way is to look for the signature splitting function $S(J)$, given in Eq. (4), to study the effect of the *cubic* term on the odd-even staggering in the γ band. The $S(J)$ is plotted as a function of the angular momentum- J as shown in Fig. 2. It is clearly seen that the sliding towards the experimental data appears when the cubic term is inserted into the EQCF Hamiltonian (2). Especially, the high levels $8_\gamma^+, 9_\gamma^+$ exactly coincide with the experimental points and this suggests that *cubic* term improves IBM-1* results.

We calculated the $B(E2)$ values by using boson effective charge $e_b = 0.097 eb$, fitted for the nuclei at $A \sim 100$ region [64]. As seen in Table 2, both results of IBM-1 and IBM-1* calculations are in good agreement with the experimental data [41]. The *cubic* term has also a positive influence on

the $B(E2)$ values.

In addition to the energy levels and $B(E2)$ values of ^{76}Se , we predicted its geometry by plotting the potential energy surface as function of deformation parameters within both formalisms in Eqs. (7) and (8). The counterplots as a function of β and γ are depicted in Fig. 3 along with its scale. Shown also is the energy surface as a function of β for $\gamma = 0^\circ$. Both plots predict the given nucleus to be spherical (using both formalisms of IBM-1 and IBM-1*). The effect of the *cubic* term is not so evident in this case, only the *second* minimum is flatter than the *first* albeit not so much.

The calculated zero value of deformation parameter using the IBM model is in contrast to the oblate deformation calculated using the RMF model [65]. The QRPA calculation of GT strength distribution is a sensitive function of the deformation parameter [37]. Table 3 shows the various values of β_2 for ^{76}Se . At the end we decided to use the β_2 value extracted from E2 transition [66] in our pn-QRPA calculation. The chosen value of β_2 was expected to give better results as it was extracted from measured data.

Fig. 4 shows cumulative GT_+ strength for ^{76}Se . Daughter excitation energy in units of MeV is represented on the abscissa. The three calculated GT_+ strength distributions include our, shell model [36] and the DQRPA [37] results. Shown also is the $^{76}\text{Se}(d, ^2\text{He})^{76}\text{As}$ experimental data of [33] and the $^{76}\text{Se}(n, p)^{76}\text{As}$ data of [34]. The (n, p) experiment performed by Helmer and collaborators resulted in two sets of data. One using the multipole decomposition analysis and the other using background subtraction technique. These are represented by EXP2 and EXP3 in Fig. 4, respectively. The figure shows very good comparison of our calculation and shell model result. The DQRPA model calculation results in largest calculated value of GT strength in ^{76}Se . There exists a considerable difference between pn-QRPA and DQRPA calculated strength distributions. We attribute this diversity to a different choice of single particle basis and interaction strength parameters. Ha & Cheoun employed a deformed, axially symmetric Woods-Saxon potential whereas we took a deformed Nilsson single particle basis. They used the Brueckner G-matrix based on the CD Bonn potential and used particle-particle and particle-hole strength parameters as $g_{pp} = 0.99$ and $g_{ph} = 1.15$. Our corresponding values were 0.04 and 0.35, respectively. Pairing gap parameter value was taken as 1.7 by Ha & Cheoun to be compared with our chosen value of 1.38. The deformation parameter β_2 adopted by Ha & Cheoun was also slightly different. They took a value of 0.3 to be compared with our value of 0.309. Our result is in decent comparison with the (d, ^2He)

data. Fig. 4 is a clear evidence of the unblocking of the GT strength. All the six measurements and calculations support the unblocking of GT strength in ^{76}Se under terrestrial conditions caused due to nuclear correlation effects. The GT strength may also be unblocked due to finite temperature effects which we discuss later.

Table 4 shows the statistics of the calculated and measured GT_+ strength distributions. Here it is noted that our model places the GT centroid at higher energy in daughter compared with the shell model calculation. The shell model calculates a slightly bigger total strength than our pn-QRPA model. It is noted that the total strength and centroid placement of the pn-QRPA calculation is in decent agreement with the measured data. It is pertinent to mention that no quenching factor was employed in shell model and DQRPA calculations.

The calculated electron capture cross section (ECC) for ^{76}Se using pn-QRPA model is shown in the Fig 5. The calculated ECC is shown as a function of temperature and incident electron energy. The threshold electron energy to initiate the electron capture process is dictated by the Q value of the nuclear reaction. The ECC increases exponentially as incident electron energy increases up to 4 MeV and later the slope decreases at high energies. This behavior maybe mapped to the trend of calculated GT distribution. States having high multipoles contribute less so the ECC increases smoothly as the incident electron energy increases. The temperature dependance of ECC is also evident from Fig 5. As the stellar temperature increases from 0.5 MeV to 1.0 MeV, one notes that the ECC increases by roughly two orders of magnitude corresponding to a significant thermal unblocking of the GT^+ channel. A further increase in temperature does not produce matching increment in the calculated ECC as majority of transitions are already thermally unblocked.

We next present the calculation of stellar electron capture rates on ^{76}Se . Fig. 6 depicts the calculated EC rates as a function of core temperature at a fixed stellar density of $10^{9.6} \text{ gcm}^{-3}$. The ordinate shows calculated EC rates in logarithmic scale having units of s^{-1} . Shown in Fig. 6 are the calculated EC rates using GT strength distributions from (i) $^{76}\text{Se}(d, ^2\text{He})^{76}\text{As}$ data [33] (marked as EXP1), (ii) shell model calculation [36] (marked as SM) and the DQRPA calculation [37]. Our calculated EC rates are calculated using first only the ground state GT strength distribution (marked as pn-QRPA(G)) and later from contribution of all excited state GT strength distributions calculated microscopically using our model and denoted by pn-QRPA(T) in

Fig. 6. In other words, apart from the pn-QRPA(T) data, all EC rates were calculated using only the ground state GT strength distribution and may be compared mutually. Our code allows manual insertion of energy levels and $B(GT)_{ij}$ strength values (see Eq. (18)). We inserted the desired experimental and theoretical data in our code to calculate the electron capture rates. We manually inserted $i = 1$ in Eq. (19) for EXP1, SM, pn-QRPA(G) and DQRPA calculated electron capture rates in our code. Here we see that the DQRPA calculated EC rates are smallest because of placement of GT centroid at much higher value (see Table 4). SM calculated EC rates are biggest. This is because SM calculated a relatively big total strength and also placed the GT centroid at relatively low energy in daughter (Table 4). At low stellar temperatures the pn-QRPA(G) and pn-QRPA(T) rates are in decent comparison with experimental data. This is because the slightly bigger centroid (calculated in the pn-QRPA model) effect is offset by the marginally bigger total strength (calculated in the pn-QRPA model). It is also noted that the pn-QRPA(G) rates are marginally bigger than the pn-QRPA(T) rates till the core temperature reaches $T_9 = 10$. This behavior is due to the fact that for the pn-QRPA(G) rates, $P_{g.s.} = 1$ (because $i = 1$). However for pn-QRPA(T) rates, $P_{g.s.} < 1$ (there are total of 180 discrete states calculated within the pn-QRPA model). At low core temperatures where the excited state occupation probability is not appreciable, the pn-QRPA(T) rates are slightly smaller than pn-QRPA(G) rates because of marginally smaller $P_{g.s.}$ value. As $T_9 \sim 10$, the partial rates from excited states contribute significantly (higher corresponding P_i values) and then total EC rates are bigger.

Next we show the same EC calculations as a function of core density and at a fixed temperature of $T_9 = 10$ (Fig. 7). Here once again the SM calculated EC rates are biggest. At high density DQRPA rates are in better agreement with EXP1 EC rates. The pn-QRPA(G) and pn-QRPA(T) rates are in decent comparison with experimental EC rates specially at low density values. It is to be noted that at a fixed temperature occupation probability of parent excited states remain constant and the variation is due to varying nature of the calculated phase space as the stellar core stiffens to higher density. We did not show the pn-QRPA calculated excited state GT strength distributions for space consideration and the same may be requested as ASCII files from the corresponding author.

Table 5 shows relative contribution of our calculated β^+ -decay and electron capture rates for ^{76}Se as a function of stellar temperature and density. The calculated EC rates are orders of magnitude bigger than the competing

β^+ -decay rates at low stellar temperatures ($T_9 \leq 5$). As the core temperature increases so does the contribution of β^+ -decay rates. In our calculation, it is assumed that at high temperatures ($kT \geq 1$ MeV), positrons appear via electron-positron pair creation process. We performed a similar study of relative contribution of β^+ -decay rates on ^{76}Se in stellar matter on a wider density range. Fig. 8 shows the EC and positron decay (PD) contribution at different $T_9(\text{K})$ temperatures and selected values of densities $10^{1.5}$, $10^{5.5}$, $10^{8.5}$ and $10^{10.5}$ gcm^{-3} . We came to the conclusion that at high stellar temperatures and low densities, the β^+ -decay on ^{76}Se may not be neglected and needs to be taken into consideration along with EC rates for better simulation results.

The energy rate of β -delayed neutron emissions at selected densities of $10^{8.5}$, $10^{9.5}$ and $10^{10.5}$ gcm^{-3} as a function of core temperature is shown in upper panel of Fig. 9. The bottom panel depicts the probability of β -delayed neutron emissions from ^{76}As (daughter of ^{76}Se). The Q-value of the reaction is -2.96058 MeV, whereas neutron separation energy of parent (daughter) nucleus used in our calculation is 11.15390 MeV (7.32861 MeV). These values were obtained using data from [54]. The energy rates of particle emission (and corresponding probability) increases with increasing density and temperature. At high stellar temperatures the rates tend to merge into each other. This is because at high stellar temperatures daughter states, with energy greater than neutron separation energy, have a finite occupation probability. The β -delayed neutron energy rate and probability of β -delayed neutron emissions merge into one another as core density stiffens from $10^{8.5}$ to $10^{10.5}$ gcm^{-3} at high T_9 values. Further at high stellar density of $10^{10.5}$ gcm^{-3} , the Fermi energy is high enough even at low temperatures and both β -delayed neutron energy rate and probability of β -delayed neutron emissions are correspondingly higher. The ASCII files of all calculated stellar rates are available and may be requested from the corresponding author.

4. Conclusion

Recently, both IBM-1 and pn-QRPA models were applied to investigate nuclear structure properties and weak rates of even-even nuclei with the same proton and neutron numbers [28, 29]. In the current work, we used two formalisms of the IBM-1 model for the description of the nuclear structure properties of ^{76}Se nucleus. We first investigated the energy levels, $B(E2)$ values and geometry of ^{76}Se within the Hamiltonian in Eqs. (2) and (3).

Later we used the pn-QRPA model to calculate GT strength distributions and associated weak-interaction mediated rates for ^{76}Se . We also commented on unblocking of GT strength in this paper.

^{76}Se exhibits typical spherical harmonic triplet (4_{gs}^+ , 2_{γ}^+ , 0_{β}^+) at low energy spectrum. Its energy ratio is $R_{4/2} = 2.38$ and is bigger than the ratio of $U(5)$ which hints that this nucleus can be located in between $U(5)$ and $O(6)$ symmetries (the spherical and the γ - softness). Therefore, we first chose the ECQF formalism in Eq. (2) that allows to move in between these symmetries. However, even-odd staggering

occurred in the γ -band levels and later we added the *cubic* term into the ECQF Hamiltonian to see the behavior of the γ - softness. Although the exact γ - softness did not appear, we obtained better results within the formalism of IBM-1* because of the effect of the *cubic* term. We analyzed the γ -band and the signatures of γ -softness by plotting the signature splitting $S(J)$ to see its effect in detail. Our calculation showed that this nucleus lies in between spherical and γ -softness transitional path. The *cubic* term had a positive effect on the γ band levels even though the energy surfaces of IBM-1 calculations resulted in a spherical minima.

In the later phase of our work we used the pn-QRPA model to calculate GT strength distributions and stellar weak rates for ^{76}Se . We decided to use the deformation value extracted from E2 transition [66] in calculation of our GT strength distribution for ^{76}Se . The choice was made due to the fact that deformation parameter is one of the key parameters in pn-QRPA calculation. As different theoretical models were suggesting varying shapes for ^{76}Se , we decided to use the value of β_2 extracted from experimental data in our pn-QRPA calculation. The energy levels for ^{76}Se , calculated by the IBM-1* model, was subsequently incorporated in the GT and weak rate calculations performed using the pn-QRPA model.

Our pn-QRPA calculation reconfirmed the unblocking of GT strength for ^{76}Se ($N > 40$ and $Z < 40$, case). The chosen β_2 value resulted in a decent comparison of calculated ground state GT strength distribution with experimental data. Later the same model was used to calculate electron capture cross sections and weak rates in stellar matter for ^{76}Se . The main feature of our calculation was a state-by-state calculation of all weak rates in a fully microscopic fashion. Our study implies that electron capture rate is the dominant mode of decay for ^{76}Se . However, at low stellar densities and high stellar temperatures, β^+ -decay on ^{76}Se should also be accounted for a better and realistic interpretation of nuclear network calculations.

Acknowledgements

J.-U. Nabi also wishes to acknowledge the support provided by the Higher Education Commission (Pakistan) through the HEC Projects No. 20-3099 and 20-5557.

References

- [1] H. A. Bethe, G. E. Brown, J. Applegate, J. M. Lattimer, Nucl. Phys. A, 324 (1979) 487.
- [2] H. A. Bethe, Rev. Mod. Phys. 62 (1990) 801.
- [3] Y. F. Niu, N. Paar, D. Vretenar, J. Meng, Phys. Rev. C 83 (2011) 045807.
- [4] N. Paar, G. Colo, E. Khan, D. Vretenar, Phys. Rev. C 80 (2009) 055801.
- [5] A. F. Fantina, E. Khan, G. Colò, N. Paar, D. Vretenar, Phys. Rev. C 86 (2012) 035805.
- [6] P. Möller, J. R. Nix, K.-L. Kratz, At. Data. Nucl. Data. Tables 66 (1997) 131.
- [7] M. Hirsch, A. Staudt, H. V. Klapdor-Kleingrothaus, At. Data. Nucl. Data. Tables 51 (1992) 243.
- [8] I. N. Borzov, Nucl. Phys. A 777 (2006) 645.
- [9] G. Martinez-Pinedo, K. Langanke, Phys. Rev. Lett. 83 (1999) 4502.
- [10] K. Langanke, D. J. Dean, P. B. Radha, Y. Alhassid, S. E. Koonin, Phys. Rev. C 52 (1995) 718.
- [11] K. Muto, E. Bender, T. Oda, Phys. Rev. C 43 (1991) 1487.
- [12] F. Iachello, A. Arima, The Interacting Boson Model, Cambridge University Press, Cambridge, 1987.
- [13] U. Kaup, C. Mönkemeyer, P. Von Brentano, Z. Phys. A 310 (1983) 129.
- [14] F. S. Radhi, N. M. Stewart, Z. Phys. A 356 (1986) 145.
- [15] K. H. Speidel, Phys. Rev. C 57 (1998) 2181.

- [16] N. Türkan, D. Olgun, I. Uluer, Cent. Eur. J. Phy 4 (2006) 124.
- [17] M. Büyükata, I. Uluer, Cent. Eur. J. Phy 6 (2008) 518.
- [18] P. O. Lipas, P. Toivonen, D. D. Warner, Phy. Lett. B 155 (1985) 295.
- [19] K. Heyde, P. V. Isacker, M. Waroquier, J. Moreau, Phy. Rev. C 29 (1984) 1420.
- [20] J. A. Halbleib, R. A. Sorenson, Nucl. Phy. A 98 (1967) 542.
- [21] D. Brink, D. Phil. Thesis, Oxford University, Unpublished 1955; P. Axel, Phys. Rev. 126 (1962) 671.
- [22] G. M. Fuller, W. A. Fowler, M. J. Newman, Astrophys. J 252 (1982) 715; G. M. Fuller, W. A. Fowler, M. J. Newman, Astrophys. J. 293 (1985) 1.
- [23] G. M. Fuller, Astrophys. J. 252 (1982) 741.
- [24] J. -U. Nabi, H. V. Klapdor-Kleingrothaus, Eur. Phys. J. A 5 (1999) 337.
- [25] J. -U. Nabi, H. V. Klapdor-Kleingrothaus, At. Data. Nucl. Data. Tables 71 (1999) 149.
- [26] J. -U. Nabi, H. V. Klapdor-Kleingrothaus, At. Data. Nuc. Data. Tables 88 (2004) 237.
- [27] K. Langanke, G. Martinez-Pinedo, Nucl. Phy. A 673 (2000) 481.
- [28] J. -U. Nabi, M. Büyükata, Nucl. Phy. A 947 (2016) 182.
- [29] J. -U. Nabi, M. Büyükata, Astrophys Space Sci. 362 (2017) 9.
- [30] K. Langanke *et al.*, Phys. Rev. Lett. 90 (2003) 241102.
- [31] R. W. Hix *et al.*, Phys. Rev. Lett. 91 (2003) 210102.
- [32] J. Cooperstein, J. Wambach, Nucl. Phys. A 420 (1984) 591.
- [33] E. W. Grewe, C. Baumer, H. Dohmann, D. Frekers, M. N. Harakeh, S. Hollstein, H. Johansson, L. Popescu, S. Rakers, D. Savran, H. Simon, J. H. Thies, A. M. Berg, H. J. Wortche, A. Zilges, Phy. Rev. C 78 (2008) 044301.

- [34] R. L. Helmer, M. A. Punyasena, R. Abegg, W. P. Alford, A. Celler, S. El-Kateb, J. Engel, D. Frekers, R. S. Henderson, K. P. Jackson, S. Long, C. A. Miller, W. C. Olsen, B. M. Spicer, A. Trudel, M. C. Vetterli, *Phys. Rev. C* 55 (1997) 6.
- [35] P. Sarriguren, E. M. D. Guerra, L. Paceaescu, A. Faessler, F. Simkovic, A. A. Raduta, *Phys. Rev. C* 67 (2003) 044313.
- [36] Q. Zhi, Y. Yu, Q. Zheng, *Chi. Phys. C* 35 (2011) 1022–1025.
- [37] E. Ha, M. K. Cheoun, *Nucl. Phys. A* 934 (2015) 73.
- [38] F. Iachello, *Lie Algebras and Applications*, Springer-Verlag, Berlin, 2006.
- [39] D. D. Warner, R. F. Casten, *Phys. Rev. Lett* 48 (1982) 1385.
- [40] D.D. Warner, R.F. Casten, *Phys. Rev. C* 28 (1983) 1798.
- [41] National Nuclear Data Center (NNDC), <http://www.nndc.bnl.gov/>, 2016.
- [42] O. Castaños, A. Frank, P. Van Isacker, *Phys. Rev. Lett.* 52 (1984) 263.
- [43] R. F. Casten, P. Von Brentano, K. Heyde, P. Van Isacker, J. Jolie, *Nucl. Phys. A* 439 (1985) 289.
- [44] R. F. Casten, P. Von Brentano, *Phys. Lett. B* 152 (1985) 22.
- [45] N. V. Zamfir, R. F. Casten, *Phys. Lett. B* 260 (1991) 265.
- [46] I. Stefanescu, A. Gelberg, J. Jolie, P. Van Isacker, P. Von Brentano, Y. X. Luod, S. J. Zhuf, J. O. Rasmussene, J. H. Hamilton, A. V. Ramayya, X. L. Che, *Nucl. Phys. A* 789 (2007) 125.
- [47] B. Sorgunlu, P. V. Isacker, *Nucl. Phys. A* 808 (2008) 27.
- [48] L. Fortunato, C. E. Alonso, J. M. Arias, J. E. García-Ramos, A. Vitturi, *Phys. Rev. C* 84 (2011) 014326.
- [49] A. E. L. Dieperink, O. Scholten and F. Iachello, *Phys. Rev. Lett.* 44 (1980) 1747.; *Nucl. Phys. A* 346 (1980) 125.

- [50] J. N. Ginocchio, M. W. Kirson, Phys. Rev. Lett. 44 (1980) 1744.; Nucl. Phys. A 350 (1980) 31.
- [51] P. Van Isacker and J.-Q. Chen, Phys. Rev. C 24 (1981) 684.
- [52] A. Bohr and B. R. Mottelson, Nuclear Structure. Volume 2: Nuclear Deformation, World Scientific Publishing, 1998.
- [53] S. G. Nilsson, Mat. Fys. Medd. Dan. Vid. Selsk 29 (1955) 16.
- [54] G. Audi, M. Wang, A. H. Wapstra, F. G. Kondev, M. MacCormick, X. Xu, B. Pfeiffer, Chin. Phys. C 36 () 1287, 2012; M. Wang, G. Audi, A. H. Wapstra, F. G. Kondev, M. MacCormick, X. Xu, B. Pfeiffer B, Chin. Phys. C 36 (2012) 1603.
- [55] N. B. Gove, M. J. Martin, Nucl. Data Tables 10 (1971) 205.
- [56] A. Jokinen, A. Nieminen, J. Äystö, R. Borcea, E. Caurier, P. Dendooven, M. Gierlik, M. Górska, H. Grawe, M. Hellström, M. Karny, Z. Janas, R. Kirchner, M. L. Compara, G. Martínez-Pinedo, P. Mayet, H. Penttilä, A. Plochocki, M. Rejmund, E. Roeckl, M. Sawicka, C. Schlegel, K. Schmidt, R. Schwengner, Eur. Phys. J. A 3 (2002) 1.
- [57] K. Nakamura, Particle Data Group, J. Phys. G. Nucl. Part. Phys. 37(7A) (2010) 075021.
- [58] S. Cakmak, J.-U. Nabi, T. Babacan, I. Maras, Adv. Space Research 55 (2015) 440.
- [59] K. Muto, E. Bender, T. Oda, H. V. Klapdor-Kleingrothaus, Z. Phys. A 341 (1992) 407.
- [60] P. C. Divari, Adv. High. Energy. Phy 2013 (2013) 11.
- [61] C. D. Goodman, C. A. Goulding, M. B. Greenfield, J. Rapaport, D. E. Bainum, C. C. Foster, W. G. Love, F. Petrovich, Phys. Rev. Lett 44 (1980) 1755.
- [62] J.-U. Nabi, A. N. Tawfik, N. Ezzelarab, A. A. Khan, Phys. Scripta 91 (2016) 055301.

- [63] R. F. Casten, Nuclear Structure From a Simple Perspective, Oxford U.P., Oxford, 1990.
- [64] M. Büyükkata, P. Van Isacker, İ. Uluer, J. Phy. G: Nucl. Part. Phy 37 (2010) 105102.
- [65] G. A. Lalazissiz, S. Raman, P. Ring, At. Data Nucl. Data Tables 71 (1999) 1.
- [66] S. Raman, C. W. Nestor, Jr., P. Tikkanen, At. Data Nucl. Data Tables 78 (2001) 1-128.

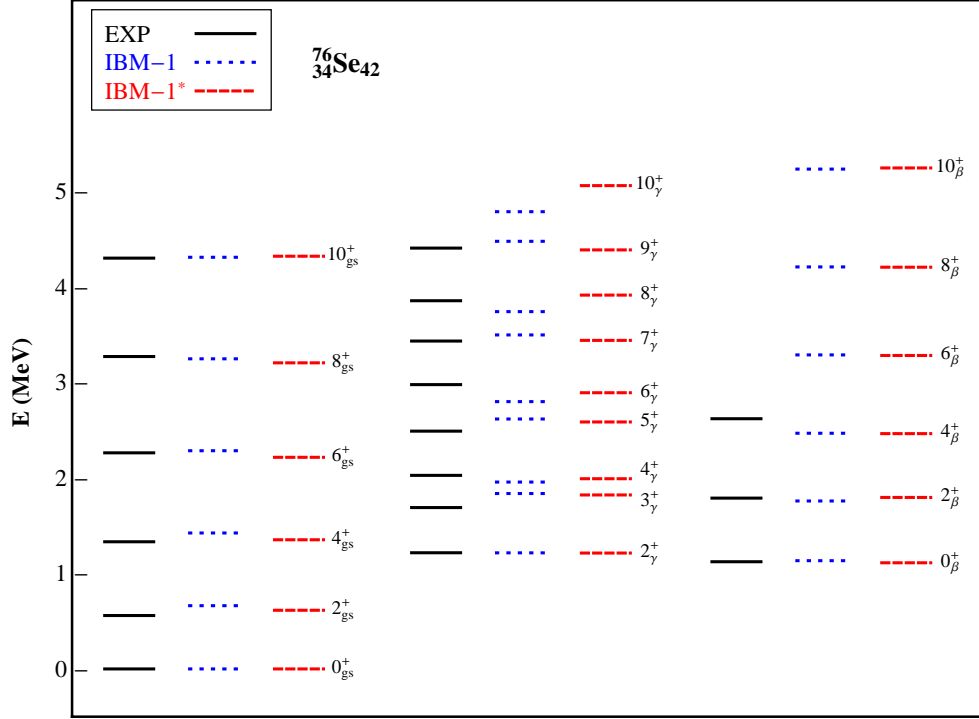


Figure 1: (Color online) The measured [41] and calculated levels for ground-state (gs), γ and β bands in the energy spectra of ^{76}Se . The bold lines indicate experimental, the dotted and dashed lines denote the calculation of IBM-1 (without *cubic* term) and IBM-1* (with *cubic* term), respectively.

Table 1: The fitted parameters of the IBM-1 Hamiltonian (Eq. (2)) in units of keV. $\bar{\chi}$ is dimensionless, N is the boson number, v_3 is the cubic interaction and σ is *rms* value.

^{76}Se	N	ϵ_d	a_1	a_2	v_3	$\bar{\chi}$	σ
IBM-1	7	524.4	14.5	5.7	-	-0.95	94
IBM-1*	7	624.9	11.6	-8.7	-81.6	-0.95	68

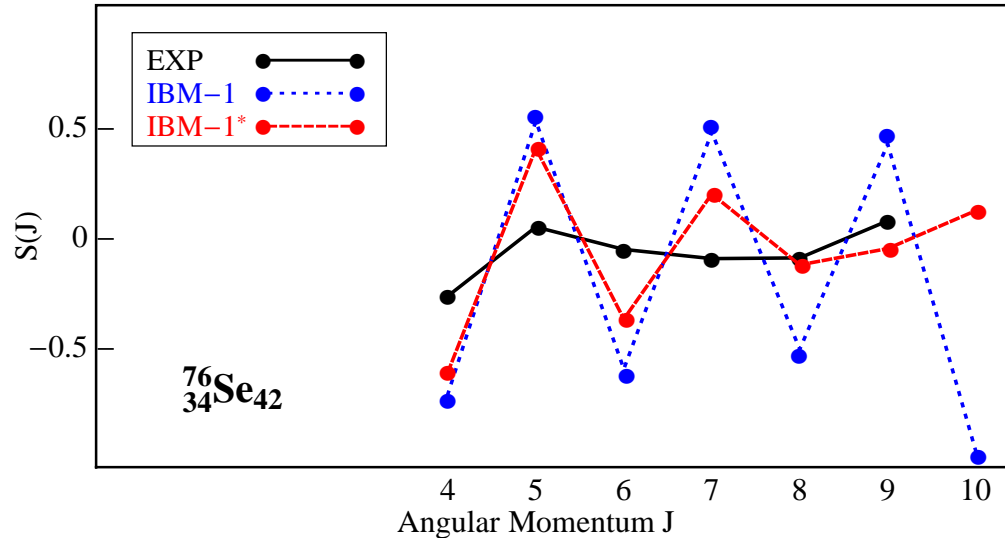


Figure 2: (Color online) The experimental (bold line) and calculated (dotted and dashed lines) odd-even staggering plots of γ bands in ^{76}Se . The exact data points of the staggering are indicated by circles; the black, blue and red ones denote the results of the experimental, IBM-1 (without *cubic* term) and IBM-1* (with *cubic* term), respectively.

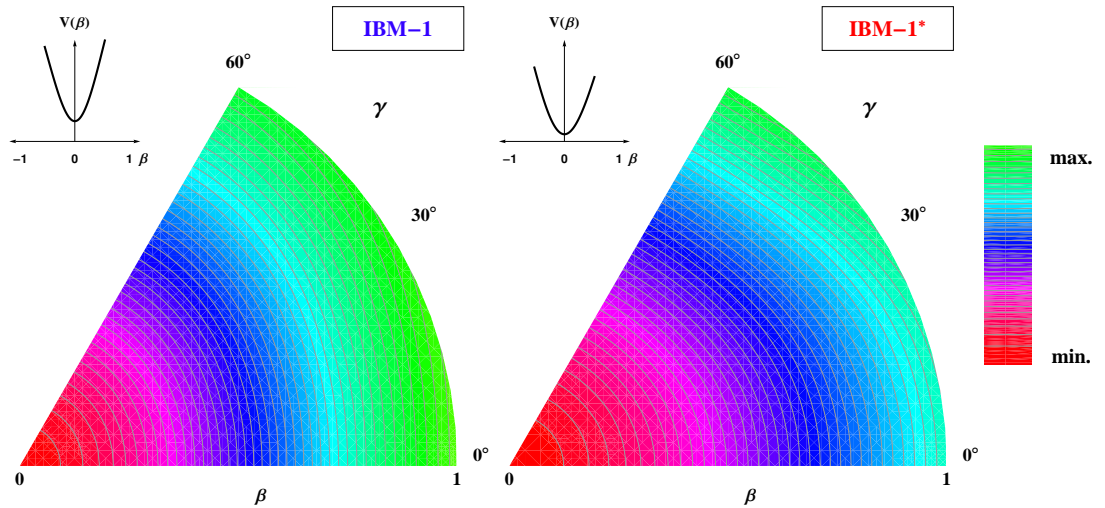


Figure 3: (Color online) Potential energy surfaces as function of β and γ for ^{76}Se nucleus and also as function of β for $\gamma = 0$.

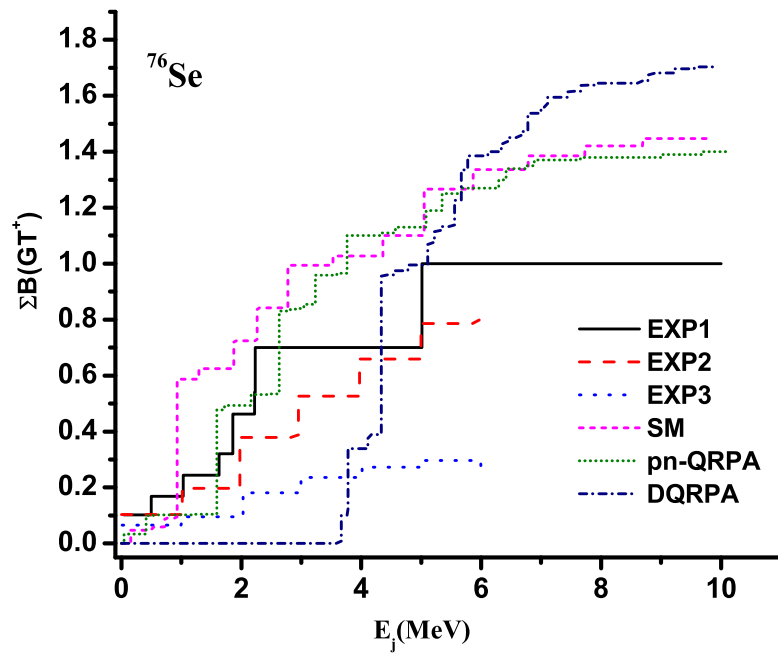


Figure 4: (Color online) Comparison of pn-QRPA calculated GT strength for ^{76}Se with experimental, shell model [36] and DQRPA model [37] results. EXP1 shows measured values by Grewe et al. [33] while EXP2 and EXP3 by Helmer et al. [34].

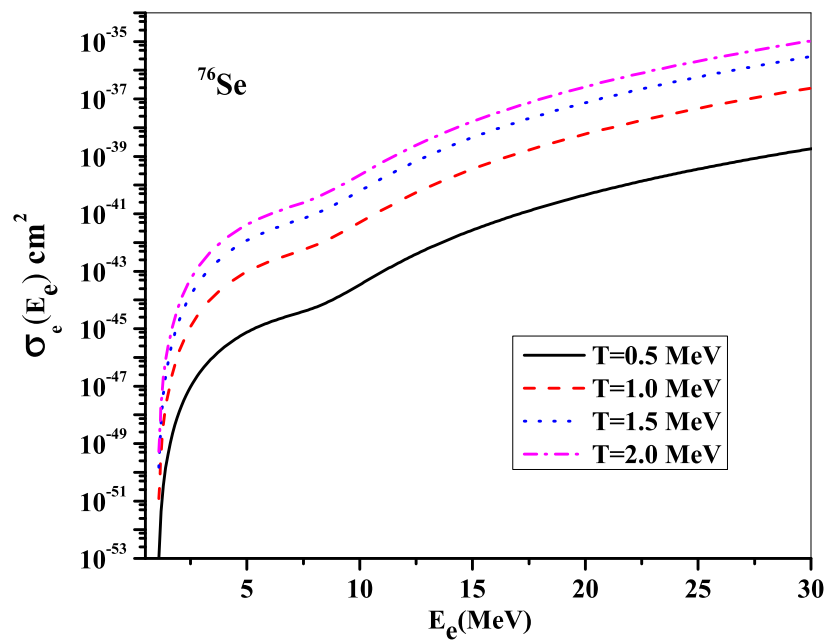


Figure 5: (Color online) The pn-QRPA calculated electron capture cross sections as a function of the incident electron energy (E_e) at different stellar temperatures.

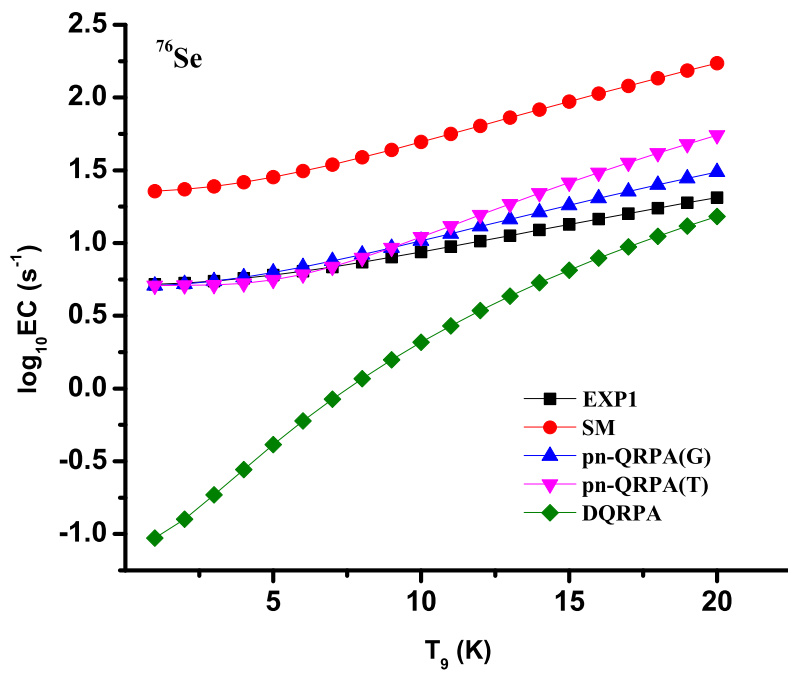


Figure 6: (Color online) Comparison of pn-QRPA calculated electron capture (EC) rates using contribution from only ground state (pn-QRPA(G)) and from all discrete excited states (pn-QRPA(T)) with EXP1 [33], shell model [36] and DQRPA [37] results, at fixed core density of $\rho = 10^{9.6} \text{ g cm}^{-3}$.

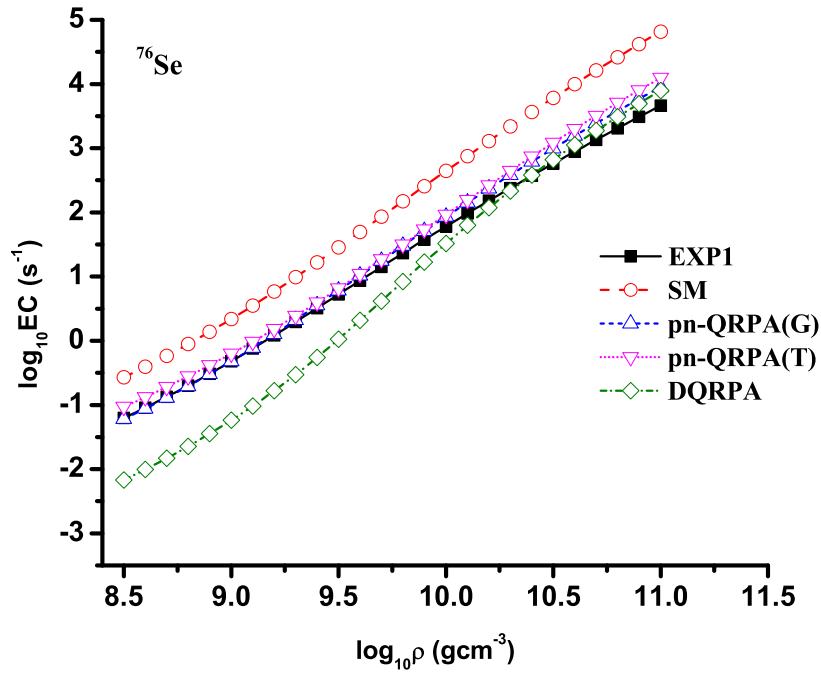


Figure 7: (Color online) Same as Fig. 6 but at fixed core temperature of $T_9(\text{K})=10$.

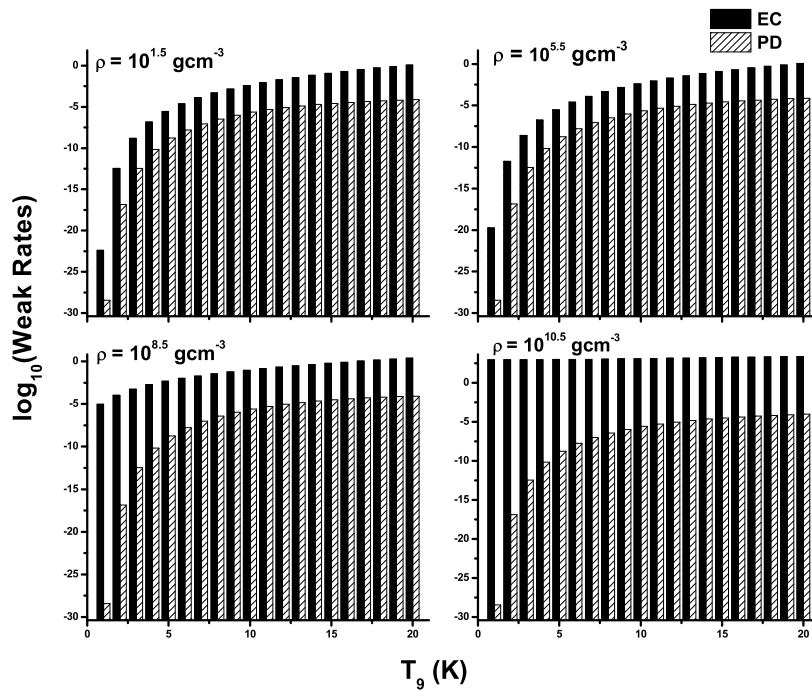


Figure 8: The pn-QRPA calculated electron capture (EC) and positron decay (PD) rates as a function of core density and temperature.

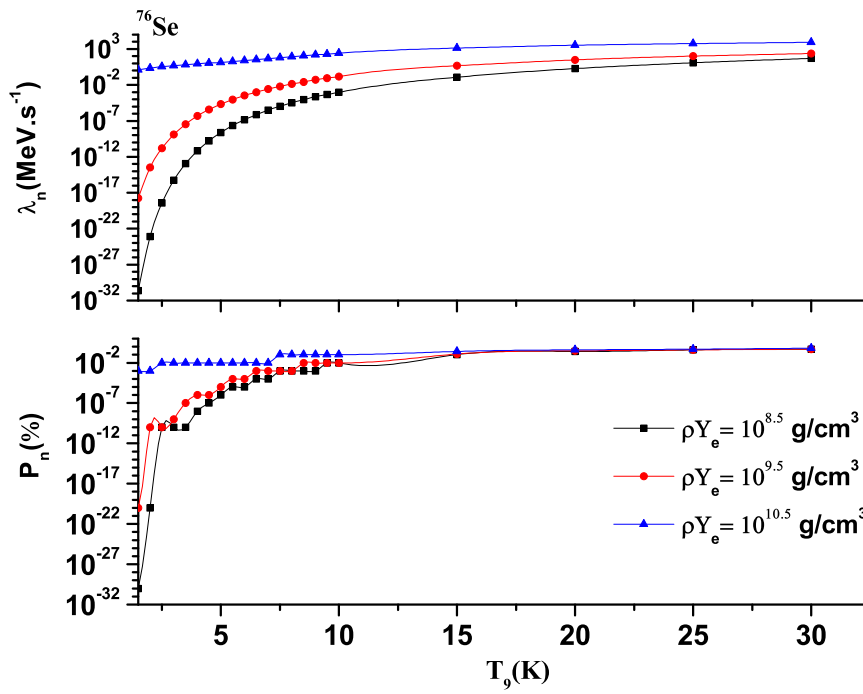


Figure 9: (Color online) Calculated β -delayed neutron energy rate (top panel) and probability of β -delayed neutron emissions (bottom panel) from ^{76}As (daughter nucleus of ^{76}Se) as a function of stellar temperature and density.

Table 2: Measured and calculated B(E2) values in units of $10^{-2} e^2 b^2$ for ^{76}Se .

$J_i^\pi \rightarrow J_f^\pi$	EXP	IBM-1	IBM-1*
$2_{gs}^+ \rightarrow 0_{gs}^+$	8.41 (<i>0.28</i>)	5.82	7.82
$4_{gs}^+ \rightarrow 2_{gs}^+$	13.58 (<i>0.55</i>)	9.97	13.41
$6_{gs}^+ \rightarrow 4_{gs}^+$	13.00 (<i>2.21</i>)	12.43	16.65
$8_{gs}^+ \rightarrow 6_{gs}^+$	15.68 (<i>4.69</i>)	13.17	17.57
$10_{gs}^+ \rightarrow 8_{gs}^+$	9.94 (<i>3.03</i>)	12.21	16.26
$2_\gamma^+ \rightarrow 0_{gs}^+$	0.23 (<i>0.03</i>)	0.005	0.02
$3_\gamma^+ \rightarrow 2_{gs}^+$	0.36 (<i>0.22</i>)	0.008	0.03
$4_\gamma^+ \rightarrow 4_{gs}^+$	4.21 (<i>1.93</i>)	6.49	6.33
$4_\gamma^+ \rightarrow 2_\gamma^+$	5.55 (<i>1.93</i>)	6.75	8.09
$5_\gamma^+ \rightarrow 3_\gamma^+$	12.81 (<i>6.34</i>)	7.36	8.58
$5_\gamma^+ \rightarrow 4_{gs}^+$	0.90 (<i>0.47</i>)	0.008	0.02
$6_\gamma^+ \rightarrow 4_\gamma^+$	5.55 (<i>4.96</i>)	9.34	11.31
$7_\gamma^+ \rightarrow 5_\gamma^+$	7.65 (<i>5.79</i>)	8.99	10.6
$0_\beta^+ \rightarrow 2_{gs}^+$	8.99 (<i>6.07</i>)	10.48	12.51

Table 3: Deformation value of ^{76}Se using RMF model [65], IBM-1 (this work) and that extracted from the E2 transition [66].

	RMF	IBM-1	E2 transition
β_2	-0.244	0.000	0.309

Table 4: Total B(GT) strengths, centroids and cut-off energy values for ^{76}Se in electron capture direction.

Model	$\sum \text{B(GT}_+)$	\bar{E}_+ (MeV)	Cut-off energy(MeV)
EXP1 [33]	1.00	2.50	10.00
EXP2 [34]	0.98	2.47	6.00
EXP3 [34]	0.35	1.16	6.00
SM [36]	1.46	2.79	9.80
pn-QRPA (this work)	1.41	3.09	12.00
DQRPA [37]	2.04	7.48	25.00

Table 5: Ratio of pn-QRPA calculated electron capture (EC) to β^+ decay rates as a function of stellar density (in units of g/cm^3) and temperature (in units of 10^9 K).

ρY_e	$R(\text{EC}/\beta^+)$			
	$T_9=1$	$T_9=5$	$T_9=10$	$T_9=20$
$10^{8.5}$	2.60E+23	2.63E+06	3.62E+04	2.98E+04
$10^{9.5}$	6.64E+28	1.60E+09	2.52E+06	4.00E+05
$10^{10.5}$	2.51E+31	5.38E+11	4.65E+08	2.50E+07